Macromolecules

Article

pubs.acs.org/Macromolecules

Does Graphene Change T_g of Nanocomposites?

Ken-Hsuan Liao,[†] Shigeru Aoyama,[†] Ahmed A. Abdala,[‡] and Christopher Macosko*,[†]

[†]Department of Chemical Engineering and Materials Science, University of Minnesota, Minneapolis, Minnesota 55455, United States

[‡]Department of Chemical Engineering, The Petroleum Institute, Abu Dhabi, United Arab Emirates

Supporting Information

ABSTRACT: The effect of the addition of graphene on the glass transition temperature (T_g) of polymers was investigated, first with poly(methyl methacrylate) and then with an extensive literature review. Isotactic (i-PMMA) and atactic PMMA (a-PMMA) were blended with pristine graphene (PG) and thermally reduced graphene (TRG). A T_g increase was found for a-PMMA nanocomposites made via *in situ* polymerization with TRG but not when a-PMMA was solvent blended with TRG. However, a T_g increase was found for TRG solvent blended into i-PMMA and a smaller increase for PG with i-PMMA. Nearly all the increase occurred at the lowest loading, 0.25 wt %, with little change at increased graphene concentration. T_g increases due to interfacial interactions between matrix polymers and fillers. Physical blending such as solvent processes cannot provide enough interaction at the interfaces, whereas chemical blending processes such as *in situ* polymerization can yield strong covalent bonds. However, i-PMMA molecules can align on graphene sheets at the interface, creating more interaction between i-PMMA and graphene than a-PMMA. Also, the T_g of i-PMMA is 60 °C lower than a-PMMA, meaning that hydrogen bonds are stronger at the lower temperature. The T_g increase of TRG/i-PMMA is higher than that of PG/i-PMMA due to more oxygen functionalities on TRG than on PG to act as interfacial interaction sites. A broad literature survey agrees with our PMMA results. We found no changes in T_g for graphene/polymer nanocomposites synthesized via physical blending processes such as solvent or melt blending, except for blending with strongly polar polymers. In contrast, chemical blending processes such as *in situ* polymerization or chemically modified fillers yielded significant T_g increases in graphene/polymer nanocomposites.

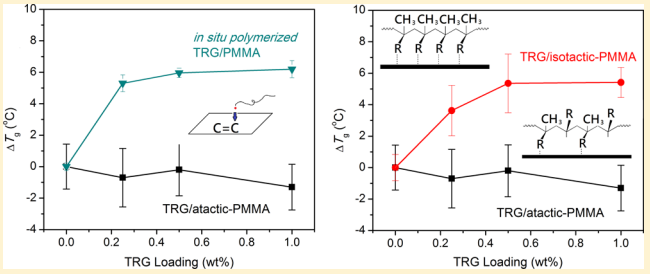

1. INTRODUCTION

It is known that near interfaces the glass transition of polymers changes. Near free surfaces it decreases, but close to strongly adsorbing surfaces it can increase significantly.[1] For example, Keddie et al.[2] reported that the T_g of atactic poly(methyl methacrylate) (a-PMMA) thin films increased on an attractive surface but decreased on a low-adhesive surface, indicating that a strong interaction between polymer and substrate can cause T_g to increase locally. These concepts have been applied to predict the T_g of polymer nanocomposites.[3−6] Ellison and Torkelson[4] reported that T_g changed near the interfaces between fillers and matrix polymers. Torkelson and co-workers used a silica/a-PMMA-thin-film/silica sandwich "model structure" to predict the T_g change of silica/PMMA nanocomposites.[6] They found that a 5 °C increase in T_g for 0.4 vol % silica particles corresponded to 130 nm thick sandwich. It is relevant to note that Grohens et al. reported that stereoregularity of PMMA had a significant influence on the T_g change.[7,8] Similar to Torkelson and others, Grohens et al. found T_g of a 35 nm atactic PMMA film increased by 8 °C on SiO_2 substrates, while for isotactic PMMA (i-PMMA) T_g increased 30 °C on SiO_2 and 40 °C on Al_2O_3. In contrast, on the same substrates T_g of syndiotactic PMMA (s-PMMA) decreased about 10 °C.

Because of its high surface area, graphene might be expected to increase the T_g of PMMA. In fact, Ramanathan et al. reported that T_g of a-PMMA increased 29 °C at 0.05 wt % of TRG.[9] However, other studies did not find any change in T_g of a-PMMA at even much higher graphene loading.[10−12] These nanocomposites were prepared by solvent blending, but a number of other studies have created graphene/PMMA composites via *in situ* polymerization of methyl methacrylate. All of these reported significant increases in T_g.[13−20]

To resolve these differences and better understand the effect of graphene on T_g, we prepared nanocomposites by both solvent blending and *in situ* polymerization. In solvent blending, to understand the role of stereoregularity, we used both i-PMMA and a-PMMA. For graphene we used thermally reduced graphene[21] (TRG; also referred to in the literature as functionalized graphene sheets or FGS). TRG has been widely used to reinforce polymers.[9,22−31] Recent studies have reported that TRG can enhance the tensile modulus of glassy polymers by 30−90% with a 2−3 vol % loading using solvent blending.[22,28] Also, to further study the effect of interfacial interactions between the matrix polymer and the filler, we dispersed nearly pristine graphene (PG) in i-PMMA for comparison to the TRG system. PG has significantly lower oxygen levels and thus should have weaker interactions at the

Received: August 30, 2014
Revised: October 28, 2014
Published: November 24, 2014

   dx.doi.org/10.1021/ma501799z | *Macromolecules* 2014, 47, 8311−8319

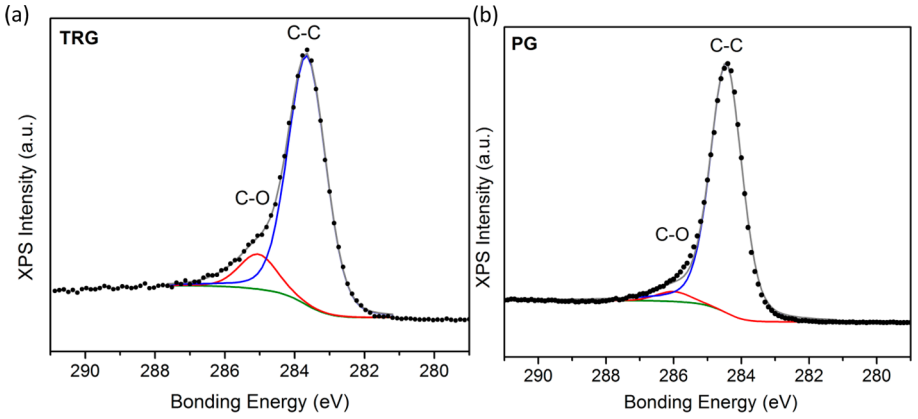

Figure 1. XPS (a) TRG and (b) PG. Carbon/oxygen atomic ratios (C/O) are 9/1 for TRG and 49/1 for PG, fitting by the Shirley–Gaussian distribution.

interfaces with PMMA due to the lack of hydroxyl and epoxy groups. We find that indeed T_g increases for composites formed via *in situ* polymerization and for solvent blending with i-PMMA but not for a-PMMA. On the basis of our PMMA results and on a review of nearly 100 papers that report T_g results for graphene/polymer nanocomposites, we propose guidelines for predicting T_g changes when graphene is added to polymers.

2. EXPERIMENTAL SECTION

2.1. Materials. The atactic PMMA (a-PMMA) was purchased from Polysciences (atactic beads, M_w = 350 000, PDI = 2.7, lot. 528266). Surfactant and other additives in the as-received a-PMMA were removed by dissolving 10 g of PMMA in 100 mL of THF and then precipitating the polymer into 300 mL of methanol (the effect of the additives in this suspension polymer is discussed further in ref 12). Isotactic PMMA (i-PMMA, Sigma-Aldrich; M_w = 64 000, PDI = 2.9), methyl methacrylate monomer (MMA; Sigma-Aldrich, 99%), *N,N*-dimethylformamide (DMF; Aldrich), tetrahydrofuran (THF; J.T. Baker), methanol (Macron), and 2,2′-azobis(2-methylpropionitrile) (AIBN; Sigma-Aldrich) were used as received.

Stereoregularity of a-PMMA and i-PMMA was confirmed using ^{1}H NMR (see Supporting Information, Figure S1), which shows that i-PMMA has mm:mr:rr = 96:3:1 and a-PMMA has mm:mr:rr = 6:38:56. The NMR results for a-PMMA and its high T_g (125 °C, Table S1) indicate that it is syndiotactic-rich.

Thermally reduced graphene sheets (TRG; Vorbeck Materials) and pristine graphene (PG; N002-PDR, Angstron Materials) were dried at 70 °C under vacuum for 24 h before use. XPS measurements were conducted on TRG and PG powders using a Surface Science SSX-100 spectrometer. Figure 1 shows a carbon/oxygen atomic ratio (C/O) of 9/1 for TRG, similar to that reported by Schneipp,[21] and 49/1 for PG. According to the manufacturer, PG is prepared by exfoliating graphite via direct ultrasonication in organic solvents without oxidation or acid-involved processes.[32]

2.2. Preparation of Nanocomposites via Solvent Blending. The solvent-blended TRG/a-PMMA and TRG/i-PMMA nanocomposites were prepared following the procedure reported by Ramanathan et al.[9] Briefly, TRG was dispersed in 10 mL of THF using a bath sonicator (Branson 2510, 100 W) at room temperature for 5 h to form a TRG/THF solution. The a-PMMA and i-PMMA were dried under vacuum at 80 °C overnight, dissolved in THF at a concentration of 10 wt % using a magnetic stirrer, and then the solution was stirred until clear (>2 h). The TRG/THF solutions were mixed with the PMMA/THF solution in varying ratios to yield approximately 1 g of total mass of TRG/PMMA with TRG loadings of 0 (control), 0.05, 0.1, 0.25, 0.5, and 1.0 wt %. All the TRG/PMMA/THF solutions were magnetically stirred for one more hour in an ice water bath. Each solution was precipitated in 300 mL of methanol, and then the precipitate was collected by vacuum filtration through a polytetrafluoroethylene (PTFE, 0.2 μm; Acrodisc CR13) membrane. The filter cakes were then dried in a vacuum oven at 80 °C for 10 h. The samples for thermomechanical and surface resistance tests were prepared from the dried filter cakes by pressing at 210 °C at 2 MPa for 5 min. PG/i-PMMA nanocomposites were produced via the same process as TRG samples.

2.3. Preparation of Nanocomposites via *in Situ* Polymerization. MMA/THF solutions were prepared at a weight ratio of MMA/THF = 2/3. TRG was then added into the 10 mL MMA/THF solutions and probe-sonicated (Cole Parmer; CPX750, 750 W) cyclically (1 s of sonication and 1 s pause) for 10 min followed by magnetic stirring for 24 h at room temperature. The TRG/MMA/THF suspensions were then purged with N_2 for 20 min prior to polymerization. AIBN was added into the purged suspensions at a weight ratio of MMA/AIBN = 1000/3, and polymerization was carried out at 65 °C for 24 h under N_2 purging. The product was precipitated by pouring the THF solution into 300 mL of methanol. The precipitate was dried after polymerization in a fume hood at 80 °C for 24 h and in a vacuum oven at 120 °C for another 24 h and then pressed at 210 °C for 5 min into films. The control group without incorporation of TRG was prepared via the same procedure.

2.4. Separation of PMMA and Graphene from Nanocomposites. The matrix PMMA of *in situ* polymerized TRG/PMMA samples was extracted. First the TRG/PMMA nanocomposites were dissolved in THF at a concentration of 10 wt %, and the black TRG/PMMA/THF solutions were filtered through a 0.2 μm filter (PTFE Acrodisc CR 13) to remove the dispersed TRG. The filtered liquids appear clear and were dried in a fume hood at 80 °C for 4 h and in a vacuum oven at 120 °C for 24 h. A clear polymer film was obtained for tests. More than 98 wt % of the PMMA matrix was recovered. Because the filtered TRG tended to stick on the PTFE filter, the TRG loaded filter was cut into small pieces and stirred vigorously in THF, which was then evaporated to recover the TRG and analyze it for bound PMMA.

2.5. Characterization of Graphene Extracted from *in Situ* Polymerized Samples. Atomic force microscopy (AFM) was used to investigate the morphology of the extracted TRG. A drop of the extracted TRG/THF solution was spin-coated on a mica substrate and air-dried at room temperature for 2 h before testing. A Digital Instrument, Nanoscope III Multimode AFM was used in noncontact mode for measurements.

Fourier transform infrared (FTIR) and Raman spectroscopy were used to investigate both TRG and the extracted graphene. TRG/THF solution and the extracted TRG/THF solution were filtered through a nylon filter (0.2 μm; Millipore GNWP) and were dried in vacuum at 40 °C for 24 h. Filtered TRG formed a paper-like structure. A Nicolet Magna-IR760 spectrometer was used to measure FTIR spectra from TRG and extracted TRG. Each TRG was ground with potassium bromide (KBr) at a mass ratio of TRG (or extracted TRG):KBr =

dx.doi.org/10.1021/ma501799z | *Macromolecules* 2014, 47, 8311–8319

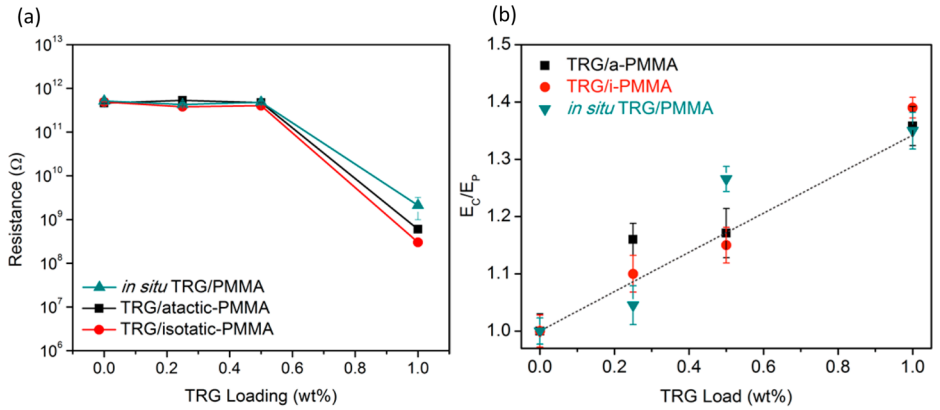

Figure 2. Comparison of TRG/i-PMMA, TRG/a-PMMA, and *in situ* TRG/PMMA nanocomposites. (a) Electrical resistances and (b) normalized storage moduli at several TRG concentrations at 25 °C. Agreement between the results indicates that a similar dispersion level of TRG was achieved in all three matrices. In (b) the dashed line is calculated assuming an aspect ratio A_f = 70 and modulus of TRG = 250 GPa.

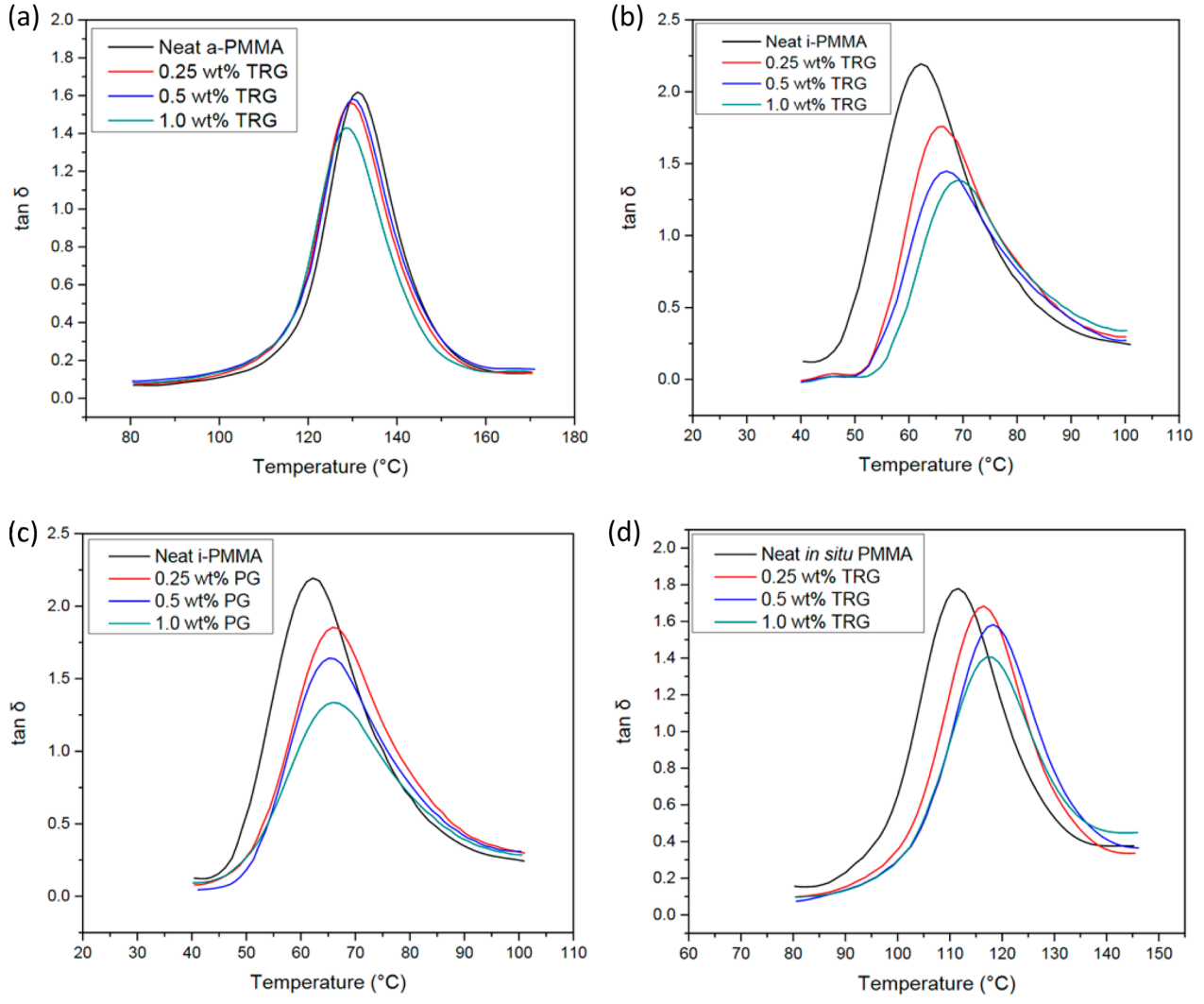

Figure 3. DMA results (tan δ) for (a) TRG/a-PMMA, (b) TRG/i-PMMA, (c) PG/i-PMMA, and (d) *in situ* TRG/PMMA nanocomposites.

1:10. Ground powders were compressed into transparent pellets for the FTIR measurements.

An alpha 300R confocal Raman microscope equipped with a UHTS200 spectrometer and a DV401 CCD detector from WITec (Ulm, Germany) was used to measure Raman spectra from graphene (TRG, PG, and extracted TRG). An air-cooled argon-ion laser operating at wavelength of 514.5 nm was used as an excitation source with the output power varying between 2 and 20 mW. A Nikon ×100 air objective was used to collect Raman spectra. Graphenes were put on a slide glass directly and set on the stage. Raman spectra from each sample were recorded with an integration time of 30−60 s at room temperature. Spectra from graphene powder were fitted by a Lorentzian function using Fityk 0.9.8 software.[33] Full width at half-maximum peak heights of the D band and of the G band were

dx.doi.org/10.1021/ma501799z | *Macromolecules* 2014, 47, 8311−8319

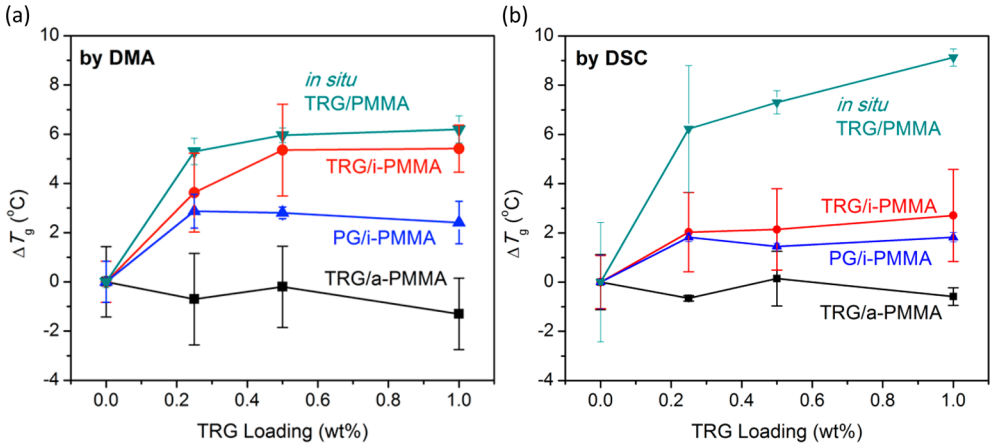

Figure 4. Summary of T_g change (ΔT_g) measured by (a) DMA, peak in tan δ and (b) DSC. Significant T_g changes were observed in TRG/i-PMMA, PG/i-PMMA, and *in situ* TRG/PMMA nanocomposites, while T_g of a-PMMA shows no significant change with incorporation of TRG.

calculated from fitting the peak profile. The peak height ratio, I_D/I_G, was also recorded.

2.6. Molecular Weight and Nanocomposite Characterization. M_w was determined using a Hewlett-Packard 1100 series liquid chromatograph fitted with a refractive index detector Hewlett-Packard 1047A) and three gel columns (500, 103, and 104 Å pore sizes; PLGel columns, PolymerLabs, Varian) with chloroform as the eluent at a flow rate of 1 mL/min at 35 °C. All the columns were calibrated with polystyrene standards (Polymer Laboratories). ^{1}H NMR was recorded on a Varian INOVA-500 spectrometer at room temperature with $CDCl_3$ as the solvent.

Differential scanning calorimeter (DSC) measurements were performed using TA Instruments Q1000 at a scan rate of 10 °C/min. The reported results were the second scan. Surface resistance of nanocomposite films was measured using an 11-probe dc resistance meter (Prostat-801). Dynamic mechanical analysis (DMA) was performed in tension at 0.5% strain and 1 rad/s at 2 °C/min using a TA Instruments RSA-G2.

FTIR and Raman spectroscopy were used to investigate the nanocomposites. A Bruker ALPHA FT-IR spectrometer in the ATR mode was used to measure FTIR spectra. Raman spectra were collected as described above. Neat PMMA sheets and graphene/PMMA nanocomposites sheets were fixed on a glass slide by double-side tape and set on the stage. Normalized spectra of graphene powder were subtracted from the obtained Raman spectra.

3. RESULTS AND DISCUSSION

3.1. Conductivity and Elastic Modulus. Conductivity and modulus were used to verify that all the TRG/PMMA nanocomposites were at the same dispersion level. Surface electrical resistance is shown in Figure 2a and Table S1 of the Supporting Information. The resistances of all three systems drop by 2 orders of magnitude at 1.0 wt % of TRG loading. The good agreement between the three samples indicates that a similar dispersion level of TRG was achieved. Estimating electrical percolation at 1.0 wt % or a volume fraction $\phi_{perc} \sim 0.004$, we can calculate an aspect ratio, A_f, for the dispersed TRG using eq 1 for randomly oriented, uniform disk-shaped particles.[27]

$$A_f = \frac{d}{h} = \frac{3\phi_{sphere}}{2\phi_{perc}} \sim 100 \quad (1)$$

where d is the diameter of the disks, h is their thickness, and $\phi_{sphere} = 0.29$, the percolation for random interpenetrating spheres.

The good agreement shown in Figure 2b and Table S1 between the normalized storage moduli (E') measured by DMA of all samples at various TRG loadings also indicates similar dispersion of TRG. We can compare these values to calculate moduli using the Mori–Tanaka model.[27,34] E' is 1 order of magnitude larger than loss modulus (E'', see Supporting Information), so E' approximately equals tensile modulus. Assuming $E' = 250$ GPa for TRG[35] and $A_f \sim 70$ gives the dashed line in Figure 2b, which is in good agreement with the experimental data. The fact that calculations using both electrical percolation and modulus values give similar aspect ratio is further indication that all TRG/i-PMMA, TRG/a-PMMA, and *in situ* TRG/PMMA nanocomposites are dispersed at a similar level.

3.2. Glass Transition Temperature. DMA results (tan δ) of the three PMMA nanocomposites prepared via solvent blending—TRG/a-PMMA, TRG/i-PMMA, and PG/i-PMMA—and via *in situ* polymerization are shown in Figure 3. Storage and loss modulus curves are shown in Figures S2 and S3 of the Supporting Information. T_g was determined from the temperature corresponding to the maximum in tan δ. The T_g values for neat a-PMMA (124.6 °C) and i-PMMA (55.7 °C) agree with the literature based on their stereoregularity.[7,8,36] T_g for the *in situ* polymerized PMMA (110.9 °C) agrees with literature values for similar free radical polymerizations at 65 °C.[13−16]

T_g of solvent-blended TRG/a-PMMA nanocomposites showed a slight decrease with incorporation of TRG, whereas TRG/i-PMMA increased by ~5 °C, PG/i-PMMA increased by ~4 °C, and *in situ* polymerized TRG/PMMA increased by ~6 °C. The T_g values at different loadings are listed in Table S1. DSC thermograms are shown in Figure S4, which are consistent with the DMA results. The changes in T_g are summarized in Figure 4. *In situ* polymerized TRG/PMMA nanocomposites show the largest T_g increase. Among the solvent-blended samples, only T_g of i-PMMA-based nanocomposites increased. More details, particularly the lack of further increase beyond 0.25 wt %, will be discussed below.

3.3. Characterization of Solvent-Blended Graphene/PMMA. To better understand the interfacial interactions that control the changes in T_g Raman spectroscopy were performed on the graphene/PMMA nanocomposites. Chen et al.[37] suggested that the peak ratio of PMMA of C–H_2 stretching (2953 cm^{-1}, I_{2953}) and C–C, C═O side chain stretching (812

dx.doi.org/10.1021/ma501799z | Macromolecules 2014, 47, 8311−8319

cm^{-1}, I_{812}) is related to the orientation of PMMA molecules at the interface between PMMA and single wall carbon nanotubes (SWCNT). A higher value of I_{2953}/I_{812} represents stronger anisotropic interactions between PMMA and SWCNT.[37]

The peak ratios (I_{2953}/I_{812}) for pure and composite samples are shown in Figure 5. The peak ratio of TRG/a-PMMA is

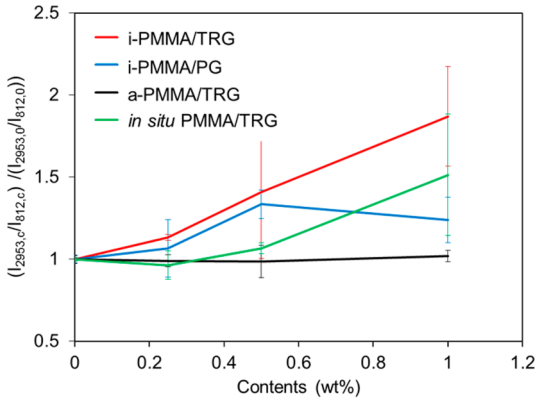

Figure 5. Raman peak ratios (I_{2953}/I_{812}) for solvent blended and *in situ* formed graphene/PMMA nanocomposites. Error bars represent range of readings from two measurements at different locations. Spectra are shown in Figure S6.

independent of graphene loading, while the peak ratios for both TRG/i-PMMA and PG/i-PMMA nanocomposites increase with higher graphene loadings. The peak ratio increase for TRG/i-PMMA is greater due to the presence of polar groups on TRG. These peak ratio results suggest that i-PMMA molecules at the interface are aligned by graphene sheets, in agreement with the Chen et al.[37] SWCNT results. Grohens et al.[7] reported that the T_g of i-PMMA thin films increased significantly when supported by aluminum or silica substrates, whereas there was no T_g change for syndiotactic-rich PMMA. They speculated that i-PMMA has a higher interaction density (i.e., more active interaction sites per chain segment) at the interfaces compared to a-PMMA.[8] Using MD simulations, Soldera et al. found that the cooperation between main chain and side chain motion of i-PMMA is higher than that of a-PMMA.[38,39] In other words, even if the numbers of hydrogen bonds between PMMA and graphene are the same, the mobility of i-PMMA molecules is more restricted than that of a-PMMA. Furthermore, it is well-known that hydrogen bonds are highly temperature-dependent. Noro and Lodge reported[40] that only 40% of the hydrogen bonds in poly(2-vinylpyridine) are active at 125 °C compared to the bonds at 65 °C.[40] In our case since i-PMMA has a T_g at 64 °C, it should have more hydrogen bonds than a-PMMA with T_g of 125 °C. Hence, isotacticity in PMMA not only increases the interaction density as Grohen et al. described[7] but also increases the hydrogen bonding interactions between graphene and PMMA. Thus, it is reasonable that our solvent blending results showing no T_g increase for the syndiotactic-rich a-PMMA but a significant increase i-PMMA with addition of pristine graphene and even more with TRG.

3.4. Investigation of *in Situ* Graphene/PMMA. *In situ* TRG/PMMA nanocomposites show a larger T_g increase than the solvent-blended TRG/i-PMMA samples (Figure 4) even though the PMMA formed *in situ* is atactic with T_g = 111 °C. The Raman peak ratios also show an increase especially at 1 wt % TRG (see Figure 5), indicating that these atactic PMMA chains are aligned on the surface of TRG.

To better understand these results, we extracted TRG from the *in situ* samples. The presence of TRG during polymerization did not affect the PMMA molecular weight. M_n was ~50 kg/mol and PDI ~2 regardless of graphene loading (Table S1). AFM images of extracted TRG showed some small spherical particles on their surfaces (Figure S5), indicating grafted PMMA. Similar AFM and TEM results were reported by Kan et al. for polymerization of glycidyl methacrylate (GMA) in the presence of graphene oxide (GO)[41] They found chemically grafted PGMA on GO surface and spheres which increased in size with longer polymerization time. Fang et al.[42] reported grafted polystyrene (PS) on GO and graphene using ATRP and observed similar spheres on GO sheets.

We used FTIR to further prove that PMMA chains were grafted to TRG (see Figure 6). Compared to pure TRG,

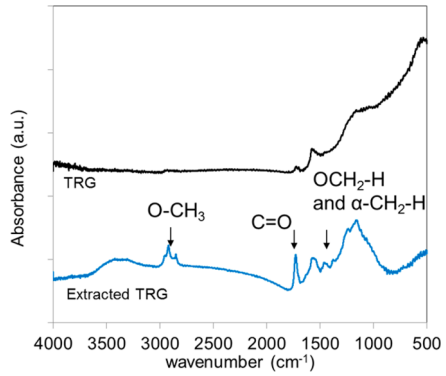

Figure 6. Fourier transform infrared spectra from TRG and TRG extracted from *in situ* polymerized PMMA.

extracted TRG has these additional vibrations: O−CH_3 (2700−3000 cm^{-1}), C═O (1727 cm^{-1}), OCH_2−H and α-CH_2−H (1430−1480 cm^{-1}).[43−45] The presence of these peaks clearly demonstrates that PMMA exists on TRG surface. Raman spectroscopy was used to determine whether the attached PMMA chains were covalently or physically bonded to TRG. The peak intensity ratio between the D-band and G-band (I_D/I_G) and peak width (full width at half-maximum, fwhm) of D-band provide information on the degree of graphitic disorder.[33,37,46,47] Raman spectra from TRG and extracted specimens are shown in Figure 7, and peak parameters of the D-band are shown in Table 1.

The fwhm of the D-band for extracted TRG is larger than for pure TRG, while the ratios of I_D/I_G for both samples are similar. This indicates that the number of sp^3-bonded carbons increased due to formation of covalent bonds between PMMA and TRG during *in situ* polymerization, in agreement with previous research. Chen et al. reported that peak width of the D-band was broadened during *in situ* polymerization of PMMA with carbon nanotubes, indicating the formation of covalent bonds between PMMA and the nanotubes.[37] Similar results were also observed for other *in situ* polymerized graphene/PMMA or GO/PMMA nanocomposites.[13−16] Kan et al. showed that free radical polymerization of vinyl monomers in the presence of GO caused polymer chains to covalently bond on GO surfaces.[41] They speculate that the loss of conjugate structure of graphene by oxidation can improve the chemical reactivity of the C═C on the sheets; hence, free radicals can attack GO or reduced GO more easily than pristine

dx.doi.org/10.1021/ma501799z | Macromolecules 2014, 47, 8311−8319

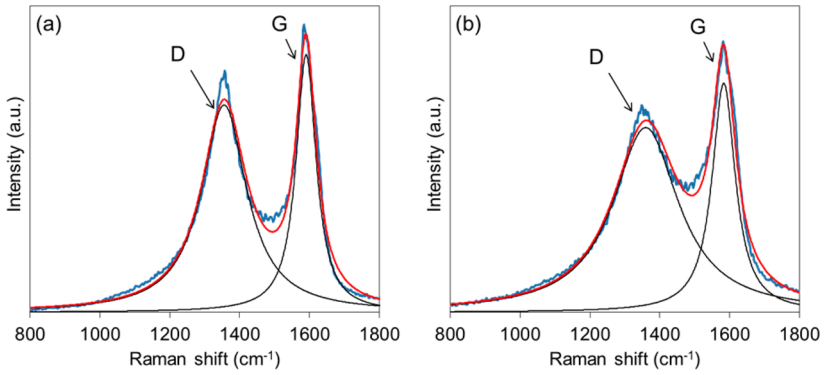

Figure 7. Raman spectra from (a) TRG and (b) TRG extracted from an *in situ* polymerized sample. Black solid lines are fits with a Lorentzian function. The red line is their summation.

Table 1. Peak Parameters of D-Band of Raman Spectra from TRG and Extracted TRG

	TRG	extracted TGR
I_D/I_G	0.84 ± 0.05	0.82 ± 0.04
fwhm (cm^{-1})	175 ± 16	225 ± 7

(dislocation-free) graphene with its perfectly conjugated structure.

Possible mechanisms for covalently bonding PMMA to the surface of graphene are shown schematically in Figure 8. Besides the reaction between free radicals on propagating chains and C═C groups on GO sheets (reaction 3 in Figure 8) that Kan et al. proposed,[41] radicals might also be generated on the surface of GO or reduced graphene by hydrogen abstraction (e.g., allyl position, olefin hydrogen). This would then be followed by (1) coupling with radicals of propagating polymer chains or (2) initiation of monomer polymerization.

To further demonstrate that PMMA covalently bonded to TRG, we compared T_g measured for *in situ* TRG/PMMA nanocomposites, extracted TRG, and the extracted matrix PMMA. Figure 9 shows that after removing the dispersed TRG, T_g decreased by ~7 °C, i.e., back to the T_g value of PMMA polymerized without TRG. We ran DSC on the extracted TRG

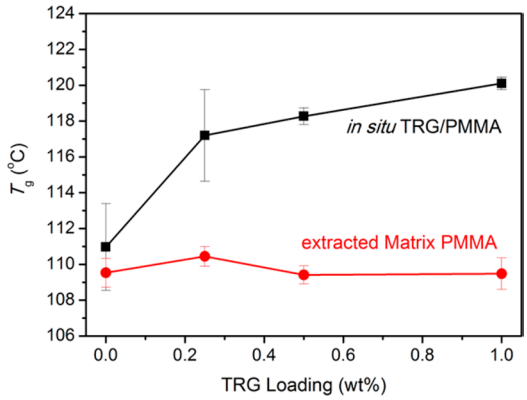

Figure 9. T_g measured by DSC of *in situ* TRG/PMMA nanocomposites and their extracted matrix PMMA.

shown in Figure 10. Although the signal is weak due the very low mass of extracted TRG, the trace indicates two T_g's. The higher T_g (142.8 °C) is ~32 °C more than the lower T_g (110.6 °C), which is same within standard deviation as PMMA polymerized without TRG (110.9 °C). The results can be explained by constrained mobility of PMMA chains covalently bonded to TRG. The lower T_g is the free matrix PMMA left

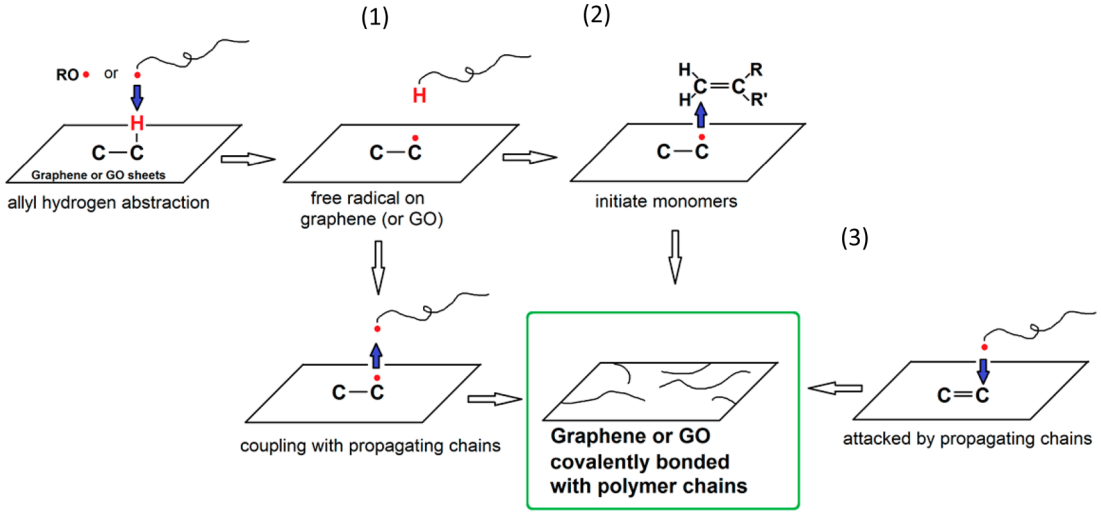

Figure 8. Three possible reactions during *in situ* polymerization in the presence of reduced graphene or GO. Hydrogen atom abstraction from GO or reduced graphene followed by (1) coupling with radicals of propagating polymer chains or (2) initiation of polymerization. (3) A free radical of a propagating polymer chain attacks a C═C bond on GO or reduced graphene sheets.

dx.doi.org/10.1021/ma501799z | *Macromolecules* 2014, 47, 8311−8319

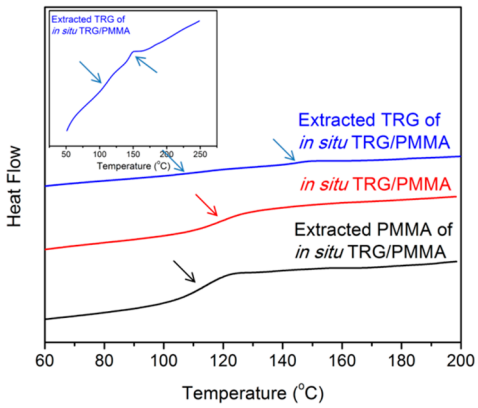

Figure 10. DSC curves of extracted TRG, matrix *in situ* PMMA, and *in situ* TRG/PMMA nanocomposites (1.0 wt %). The inset is the DSC curve of extracted TRG on a much expanded scale.

over after washing. As reported in the Experimental Section, the extracted matrix polymer occupied >98 wt % of the original nanocomposites, indicating only small amount of PMMA is covalently bonded to TRG. Yet this small amount seems to be responsible for the increase in T_g of the *in situ* graphene/PMMA nanocomposites.

We need to explain how such small amounts of covalently bonded chains can lead to the increase in T_g. Moreover, why does T_g not increase linearly, but appears to plateau at low graphene loadings, as shown in Figures 4 and 9? The answer to both questions lies in the effect of chain confinement. Torkelson and co-workers showed that attractive surfaces can restrict the mobility of polymer chains for hundreds of nanometers.[4,6] For example, they found the T_g of a 130 nm thick layer of PMMA increased 5 °C when confined between two silica sheets.[6] We can use this result with a simple calculation to show that nearly all our PMMA could be confined with the addition of only 0.5 wt % TRG. If we assume perfectly dispersed, single layers of graphene, h = 0.345 nm, which are large in diameter such that we can neglect their edges, we obtain a relation between the volume fraction of confined polymer, $\phi_{confine}$, and volume fraction of graphene, ϕ_G, and the confinement length, L.

$$\phi_{confine} = \phi_G \frac{h + L}{h} \tag{2}$$

Using a density of 2.25 for TRG and 1.18 for PMMA, 0.5 wt % TRG gives ϕ_G = 0.0024. With L = 130 nm gives $\phi_{confine}$ = 0.89. Thus, increasing loading beyond 0.5 wt % is not expected to increase confinement significantly, consistent with the plateauing in T_g with graphene loading that we observe. Torkelson and co-workers also found a plateau in T_g values at low loading of silica nanoparticles.[6] And what about the role of the covalently bonded chains? In Figure 4 there is no increase in T_g when TRG is solvent-blended into a-PMMA. However, when PMMA chains are covalently bonded to the graphene surface, they become highly immobilized as demonstrated by the 32 °C increase in T_g shown in Figure 10. These chains have a strong influence on their unattached neighbors, leading to the overall increase in T_g of 6–9 °C.

4. REVIEW OF LITERATURE ON THE EFFECT OF GRAPHENE ON T_g OF MATRIX POLYMERS

A broad literature review of the thermal properties of graphene/polymer nanocomposites is presented in the tables in the Supporting Information. These are arranged by method of formation: solvent blending (Tables S2 and S3), melt blending (Table S4), *in situ* polymerization (Table S5), and chemically modified graphene (Table S6). Definitions of the abbreviations are given after Table S6.

In Tables S2 and S4, 30 of the 33 papers describing graphene/polymer nanocomposites prepared via solvent or melt blending show no significant T_g change as measured by DMA or DSC. One of the exceptions was Ramanathan et al.[9] for PMMA. We have repeated their experiments using the same a-PMMA and found no T_g increase. Liao et al. have shown that most likely Ramanathan et al. did not remove surfactants and other additives from their starting a-PMMA, which led to an artificially low T_g of their control.[12] The results summarized in Tables S2 and S4 indicate that solvent and melt blending processes do not provide enough interaction between matrix polymers and graphene or graphene oxide (GO) fillers, leading to little or no T_g change.

Table S5 shows graphene/polymer nanocomposites prepared via *in situ* polymerization with unmodified graphene while Table S6 shows T_g results for samples made by solvent blending with chemically modified graphene or graphene oxide. Of 62 papers, 50 report T_g increases of 4 °C or more. Several of the studies in Table S5 that showed no increase with *in situ* polymerization used pristine graphene. We speculate that the pristine graphene's conjugated C=C is too chemically stable to react with the propagating free radical and hence provides no covalent bonding between graphene and the matrix polymer. Several studies in Table S6 involve covalently bonding short polymer chains on the fillers' surfaces prior to the blending process to enhance compatibility; hence, even solvent-blending these modified graphene or GO in polymers can cause significant T_g increase. Our work with *in situ* polymerization of PMMA described above shows that the strong interfacial interactions from covalent bonded chains can affect neighboring chains and raise the T_g of nanocomposites.

Table S3 shows GO blended with water-soluble polymers. All except chitosan show a significant T_g increase even though there is no covalent bonding. We speculate that strong hydrogen bonds were formed between polymers and GO via the simple aqueous blending process. In such systems, a high level of hydrogen bonding is expected due to not only the nature of the water-soluble polymers but also the higher content of oxygen groups in GO (C/O = 2) compared to TRG and CRG (C/O ratio ≫ 9/1). This interesting phenomenon further supports our previous conclusion that interaction between matrix polymers and graphene is the primary cause of T_g increase. However, it is useful to point out that hydrogen bonds will be weakened at temperatures higher than 100 °C. As such, reports with a matrix polymer's T_g much higher than 100 °C should use caution in attributing the T_g increase to hydrogen bonds. For example, GO/chitosan nanocomposites with a matrix polymer T_g at 175 °C resulted in a T_g increase of only 5 °C.[48] Some of this increase may be due to electrostatic attraction immobilizing the chitosan chains.[49,50]

dx.doi.org/10.1021/ma501799z | *Macromolecules* 2014, 47, 8311–8319

5. CONCLUSIONS

The influence of graphene on T_g was investigated in this work. We used isotactic PMMA (i-PMMA) and syndiotactic-rich, atactic PMMA (a-PMMA) as matrix polymers and thermally reduced graphene (TRG) and nearly pristine graphene (PG) as graphene fillers for investigation. Graphene/PMMA nanocomposites were prepared by two methods: *in situ* polymerization and solvent blending. The effect of these processing methods and PMMA tacticity on T_g was investigated. A T_g increase was found in solvent-blended TRG/i-PMMA, PG/i-PMMA, and *in situ* polymerized TRG/PMMA nanocomposites, but not in solvent-blended TRG/a-PMMA nanocomposites. Additionally, the T_g increase of TRG/i-PMMA was higher than that of PG/i-PMMA. The results can be explained by the difference levels of matrix polymer immobilization at the graphene interface. *In situ* polymerized TRG/PMMA nanocomposites show a larger T_g increase than all solvent-blended graphene/PMMA nanocomposites because a portion of the matrix PMMA covalently bonded to TRG. T_g increase of solvent-blended graphene/i-PMMA nanocomposites can be attributed to immobilization of matrix i-PMMA molecules, which is affected by (i) conformation of i-PMMA at interface, (ii) interaction density between PMMA and graphene, and (iii) the low T_g of i-PMMA. Alignment of i-PMMA molecules at the graphene interface creates more interaction between i-PMMA and graphene than a-PMMA. TRG with lower C/O ratio (more oxygen atoms) than PG provides more interaction with i-PMMA and causes a larger T_g increase than PG, while TRG/a-PMMA nanocomposites do not show any T_g change.

These experimental results combined with an extensive literature summary show that the T_g of graphene or GO/polymer nanocomposites can be increased only if strong interactions are formed between matrix polymers and fillers. Blending processes, such as solvent and melt blending which do not involve covalent bonding to the graphene surface, are generally incapable of providing enough restriction by interactions between the matrix polymers and fillers. However, the chains of polar polymers with low T_g can be confined by strong hydrogen bonding to graphene containing oxygen groups (TRG, CRG, and GO); they typically show a T_g increase. Blending processes involving chemical reactions, such as chemically modified graphene or *in situ* polymerization of monomers in the presence of TRG, CRG, or GO, are capable of providing strong confinement by covalent bonds between matrix polymers and fillers. One exception is *in situ* polymerized monomers in the presence of pristine graphene, which showed no T_g change of the resulting nanocomposites.[51] This was because no oxidized functional groups or reactive C=C exist on pristine graphene surface for the monomer to chemically react with.

■ ASSOCIATED CONTENT

Supporting Information

Experimental details including NMR spectra, E' and E'' vs temperature; DSC scans, AFM images, and Raman spectra; table with properties of all nanocomposites samples; five tables of T_g values from the literature. This material is available free of charge via the Internet at http://pubs.acs.org.

■ AUTHOR INFORMATION

Corresponding Author

*E-mail: macosko@umn.edu (C.M.).

Present Addresses

A.A.A.: Department of Petroleum Refining and Chemical Engineering, Suez University, Suez, Egypt.

K.-H.L.: DuPont Central Research & Development, Experimental Station, Wilmington, DE.

S.A.: Toray Industries, Inc., Otsu, Shiga, Japan.

Notes

The authors declare no competing financial interest.

■ ACKNOWLEDGMENTS

The authors acknowledge the financial support from the Abu Dhabi-Minnesota Institute for Research Excellence (ADMIRE), a partnership between the Petroleum Institute of Abu Dhabi and the Department of Chemical Engineering and Materials Science at the University of Minnesota. The authors also thank Jerry Yeh for his help with DSC and DMA measurements and in documentation. This work utilized the University of Minnesota College of Science and Engineering Characterization Facility, which received partial support from the NSF-NNIN program and capital equipment funding from the NSF through the MRSEC program.

■ REFERENCES

(1) Li, X.; McKenna, G. B. Considering viscoelastic micromechanics for the reinforcement of graphene polymer nanocomposites. *ACS Macro Lett.* **2012**, *1*, 388−391.

(2) Keddie, J. L.; Jones, R. A. L.; Cory, R. A. Interface and surface effects on the glass-transition temperature in thin polymer films. *Faraday Discuss.* **1994**, *98*, 219.

(3) Bansal, A.; Yang, H.; Li, C.; Cho, K.; Benicewicz, B. C.; Kumar, S. K.; Schadler, L. S. Quantitative equivalence between polymer nanocomposites and thin polymer films. *Nat. Mater.* **2005**, *4*, 693−698.

(4) Ellison, C. J.; Torkelson, J. M. The distribution of glass-transition temperatures in nanoscopically confined glass formers. *Nat. Mater.* **2003**, *2*, 695−700.

(5) Schadler, L. Nanocomposites: Model interfaces. *Nat. Mater.* **2007**, *6*, 257−258.

(6) Rittigstein, P.; Priestley, R. D.; Broadbelt, L. J.; Torkelson, J. M. Model polymer nanocomposites provide an understanding of confinement effects in real nanocomposites. *Nat. Mater.* **2007**, *6*, 278−282.

(7) Grohens, Y.; Hamon, L.; Reiter, G.; Soldera, A.; Holl, Y. Some relevant parameters affecting the glass transition of supported ultra-thin polymer films. *Eur. Phys. J. E: Soft Matter* **2002**, *8*, 217−224.

(8) Grohens, Y.; Brogly, M.; Labbe, C.; David, M.-O.; Schultz, J. Glass transition of stereoregular poly(methyl methacrylate) at interfaces. *Langmuir* **1998**, *14*, 2929−2932.

(9) Ramanathan, T.; et al. Functionalized graphene sheets for polymer nanocomposites. *Nat. Nanotechnol.* **2008**, *3*, 327−331.

(10) Wallin, T. *Mechanical Properties of Polymer Nanocomposites Based on Functionalized Graphene Sheets*; Senior Thesis, College of William and Mary: 2010.

(11) Vleminckx, G.; et al. Effect of thermally reduced graphene sheets on the phase behavior, morphology, and electrical conductivity in poly[(α-methyl styrene)-co-(acrylonitrile)/poly(methyl-methacrylate) blends. *ACS Appl. Mater. Interfaces* **2011**, *3*, 3172−3180.

(12) Liao, K.-H.; Kobayashi, S.; Kim, H.; Abdala, A. A.; Macosko, C. W. Influence of functionalized graphene gheets on the modulus and glass transition of PMMA. *Macromolecules* **2014**, *47*, 7674−7676.

(13) Potts, J. R.; et al. Thermomechanical properties of chemically modified graphene/poly(methyl methacrylate) composites made by in situ polymerization. *Carbon* **2011**, *49*, 2615−2623.

(14) Wang, J.; et al. Preparation and mechanical and electrical properties of graphene nanosheets-poly(methyl methacrylate) nano-

composites via in situ suspension polymerization. *J. Appl. Polym. Sci.* **2011**, *122*, 1866−1871.
(15) Jang, J. Y.; Jeong, H. M.; Kim, B. K. Compatibilizing effect of graphite oxide in graphene/PMMA nanocomposites. *Macromol. Res.* **2009**, *17*, 626−629.
(16) Jang, J.; Kim, M.; Jeong, H.; Shin, C. Graphite oxide/poly(methyl methacrylate) nanocomposites prepared by a novel method utilizing macroazoinitiator. *Compos. Sci. Technol.* **2009**, *69*, 186−191.
(17) Pramoda, K. P.; Hussain, H.; Koh, H. M.; Tan, H. R.; He, C. B. Covalent bonded polymer-graphene nanocomposites. *J. Polym. Sci., Part A: Polym. Chem.* **2010**, *48*, 4262−4267.
(18) Bian, J.; et al. Fabrication of microwave exfoliated graphite oxide reinforced thermoplastic polyurethane nanocomposites: Effects of filler on morphology, mechanical, thermal and conductive properties. *Composites, Part A* **2013**, *47*, 72−82.
(19) Aldosari, M.; Othman, A.; Alsharaeh, E. Synthesis and characterization of the in situ bulk polymerization of PMMA containing graphene sheets using microwave irradiation. *Molecules* **2013**, *18*, 3152−3167.
(20) Morimune, S.; Nishino, T.; Goto, T. Ecological Approach to graphene oxide reinforced poly(methyl methacrylate) nanocomposites. *ACS Appl. Mater. Interfaces* **2012**, *4*, 3596−3601.
(21) Schniepp, H. C.; et al. Functionalized single graphene sheets derived from splitting graphite oxide. *J. Phys. Chem. B* **2006**, *110*, 8535−8539.
(22) Steurer, P.; Wissert, R.; Thomann, R.; Mülhaupt, R. Functionalized graphenes and thermoplastic nanocomposites based upon expanded graphite oxide. *Macromol. Rapid Commun.* **2009**, *30*, 316−327.
(23) Kim, H.; Abdala, A. A.; Macosko, C. W. Graphene/polymer nanocomposites. *Macromolecules* **2010**, *43*, 6515−6530.
(24) Das, B.; Eswar Prasad, K.; Ramamurty, U.; Rao, C. N. R. Nano-indentation studies on polymer matrix composites reinforced by few-layer graphene. *Nanotechnology* **2009**, *20*, 125705.
(25) Verdejo, R.; Barroso-Bujans, F.; Rodriguez-Perez, M. A.; Antonio de Saja, J.; Lopez-Manchado, M. A. Functionalized graphene sheet filled silicone foam nanocomposites. *J. Mater. Chem.* **2008**, *18*, 2221.
(26) Kim, H.; Macosko, C. W. Processing-property relationships of polycarbonate/graphene composites. *Polymer* **2009**, *50*, 3797−3809.
(27) Kim, H.; Macosko, C. W. Morphology and properties of polyester/exfoliated graphite nanocomposites. *Macromolecules* **2008**, *41*, 3317−3327.
(28) Ansari, S.; Giannelis, E. P. Functionalized graphene sheet-poly(vinylidene fluoride) conductive nanocomposites. *J. Polym. Sci., Part B: Polym. Phys.* **2009**, *47*, 888−897.
(29) Nguyen, D. A.; et al. Morphological and physical properties of a thermoplastic polyurethane reinforced with functionalized graphene sheet. *Polym. Int.* **2009**, *58*, 412−417.
(30) Rafiee, M. A.; et al. Enhanced mechanical properties of nanocomposites at low graphene content. *ACS Nano* **2009**, *3*, 3884−3890.
(31) Kim, H.; Miura, Y.; Macosko, C. W. Graphene/polyurethane nanocomposites for improved gas barrier and electrical conductivity. *Chem. Mater.* **2010**, *22*, 3441−3450.
(32) Zhamu, A.; Jang, B. Mass production of pristine nano graphene materials, Patent US8226801, 2012.
(33) Chieu, T.; Dresselhaus, M.; Endo, M. Raman studies of benzene-derived graphite fibers. *Phys. Rev. B* **1982**, *26*, 5867−5877.
(34) Tandon, G. P.; Weng, G. J. The effect of aspect ratio of inclusions on the elastic properties of unidirectionally aligned composites. *Polym. Compos.* **1984**, *5*, 327−333.
(35) Suk, J. W.; Piner, R. D.; An, J.; Ruoff, R. S. Mechanical properties of monolayer graphene oxide. *ACS Nano* **2010**, *4*, 6557−6564.
(36) *Polymer Handbook*; Wiley: New York, 1999.
(37) Chen, B.; et al. Modifying the electronic character of single-walled carbon nanotubes through anisotropic polymer interaction: a Raman study. *Adv. Funct. Mater.* **2005**, *15*, 1183−1187.
(38) Soldera, A.; Grohens, Y. Local dynamics of stereoregular PMMAs using molecular simulation. *Macromolecules* **2002**, *35*, 722−726.
(39) Soldera, A.; Grohens, Y. Cooperativity in stereoregular PMMAs observed by molecular simulation. *Polymer* **2004**, *45*, 1307−1311.
(40) Noro, A.; Matsushita, Y.; Lodge, T. P. Thermoreversible supramacromolecular ion gels via hydrogen bonding. *Macromolecules* **2008**, *41*, 5839−5844.
(41) Kan, L.; Xu, Z.; Gao, C. General avenue to individually dispersed graphene oxide-based two-dimensional molecular brushes by free radical polymerization. *Macromolecules* **2011**, *44*, 444−452.
(42) Fang, M.; Wang, K.; Lu, H.; Yang, Y.; Nutt, S. Single-layer graphene nanosheets with controlled grafting of polymer chains. *J. Mater. Chem.* **2010**, *20*, 1982.
(43) Willis, H. .; Zichy, V. J. .; Hendra, P. . The laser-Raman and infra-red spectra of poly(methyl methacrylate). *Polymer* **1969**, *10*, 737−746.
(44) Schmidt, P.; Schneider, B.; Dirlikov, S.; Mihailov, M. Temperature changes of infra-red bands of poly(methyl methacrylate). *Eur. Polym. J.* **1975**, *11*, 229−232.
(45) Dybal, J.; Štokr, J.; Schneider, B. Vibrational spectra and structure of stereoregular poly(methyl methacrylates) and of the stereocomplex. *Polymer* **1983**, *24*, 971−980.
(46) Subrahmanyam, K. S.; Vivekchand, S. R. C.; Govindaraj, A.; Rao, C. N. R. A study of graphenes prepared by different methods: characterization, properties and solubilization. *J. Mater. Chem.* **2008**, *18*, 1517.
(47) Calderon Moreno, J. M.; Swamy, S. S.; Fujino, T.; Yoshimura, M. Carbon nanocells and nanotubes grown in hydrothermal fluids. *Chem. Phys. Lett.* **2000**, *329*, 317−322.
(48) Yang, X.; Tu, Y.; Li, L.; Shang, S.; Tao, X. Well-dispersed chitosan/graphene oxide nanocomposites. *ACS Appl. Mater. Interfaces* **2010**, *2*, 1707−1713.
(49) Leszczynska, A.; Pielichowski, K. Application of thermal analysis methods for characterization of polymer/montmorillonite nanocomposites. *J. Therm. Anal. Calorim.* **2008**, *93*, 677−687.
(50) Yao, Z.; Braidy, N.; Botton, G. A.; Adronov, A. Polymerization from the surface of single-walled carbon nanotubes − Preparation and characterization of nanocomposites. *J. Am. Chem. Soc.* **2003**, *125*, 16015−16024.
(51) Wang, X. W.; et al. Enhanced performance of biodegradable poly(butylene succinate)/graphene oxide nanocomposites via *in situ* polymerization. *Langmuir* **2012**, *28*, 7091−7095.